Elsevier Editorial System(tm) for Journal of Pharmaceutical and Biomedical Analysis
Manuscript Draft

Manuscript Number: JPBA-D-14-00875R1

Title: METABOLOMIC SCREENING OF REGIONAL BRAIN ALTERATIONS IN THE APP/PS1 TRANSGENIC MOUSE MODEL OF ALZHEIMER'S DISEASE BY DIRECT INFUSION MASS SPECTROMETRY

Article Type: Full Length Article

Keywords: Metabolomics; APP/PS1 mice; brain regions; direct infusion mass spectrometry; Alzheimer's disease

Corresponding Author: Prof. JOSE LUIS GOMEZ-ARIZA, Ph.D.

Corresponding Author's Institution: UNIVERSITY OF HUELVA

First Author: Raul Gonzalez-Dominquez, Ms

Order of Authors: Raul Gonzalez-Dominquez, Ms; Tamara Garcia-Barrera, Ph. Dr.; Javier Vitorica, Ph. Dr.; JOSE LUIS GOMEZ-ARIZA, Ph.D.

Abstract: The identification of pathological mechanisms underlying to Alzheimer's disease is of great importance for the discovery of potential markers for diagnosis and disease monitoring. In this study, we investigated regional metabolic alterations in brain from the APP/PS1 mice, a transgenic model that reproduces well some of the neuropathological and cognitive deficits observed in human Alzheimer's disease. For this purpose, hippocampus, cortex, cerebellum and olfactory bulbs were analyzed using a high-throughput metabolomic approach based on direct infusion mass spectrometry. Metabolic fingerprints showed significant differences between transgenic and wild-type mice in all brain tissues, being hippocampus and cortex the most affected regions. Alterations in numerous metabolites were detected including phospholipids, fatty acids, purine and pyrimidine metabolites, acylcarnitines, sterols and amino acids, among others. Furthermore, metabolic pathway analysis revealed important alterations in homeostasis of lipids, energy management, and metabolism of amino acids and nucleotides. Therefore, these findings demonstrate the potential of metabolomic screening and the use of transgenic models for understanding pathogenesis of Alzheimer's disease.

Suggested Reviewers:

Dear Editor,

Please find enclosed the manuscript “METABOLOMIC SCREENING OF REGIONAL BRAIN ALTERATIONS IN THE APP/PS1 TRANSGENIC MOUSE MODEL OF ALZHEIMER’S DISEASE BY DIRECT INFUSION MASS SPECTROMETRY" by R. González-Domínguez, T. García-Barrera, J. Vitorica and J.L. Gómez-Ariza, to be published in Journal of Proteomics.

This work considers the application for the first time of direct infusion electrospray mass spectrometry for the study of metabolic abnormalities in different brain regions of the APP/PS1 transgenic mice, including cortex, hippocampus, cerebellum and olfactory bulbs. Multivariate statistics demonstrated the potential of high-throughput fingerprinting for the discrimination between transgenic animals and wild-type controls, and indicated that pathological processes are widespread and not only affect to hippocampus and cortex, primary targets in Alzheimer’s disease. Furthermore, numerous metabolites were identified as potential markers of AD-type disorders in these mice, which may contribute to deepen into underlying pathological mechanisms related to neurodegenerative processes.

Therefore, these results highlight the importance of transgenic models for the study of underlying pathological mechanisms in AD brain, a sample not readily accessible in human investigations.

Sincerely yours,

José Luis Gómez Ariza

Combined Reviewers' comments:

Compound Identification:

1. Direct infusion mass spectrometry lacks of the information provided by retention time and the resolution of different signals for different compounds. In this scenario the authors say: (line 138) "For this, the peak search was done with a mass tolerance of 0.1Da, and a minimum response of 10 counts was considered for filtering".

The above error in mass means working with nominal mass more than exact mass and the level of signal means accepting even noise as a signal. Any information obtained under those conditions is doubtful. It is true that they can confirm some lipids through positive and negative ionization modes and with the fragments, but any other compound is in my opinion just an educated guess.

The "mass tolerance of 0.1Da" mentioned in line 138 refers to the m/z width used for data filtering (not mass accuracy). Data filtering in metabolomics based on direct infusion with TOF-MS is usually performed following the procedure employed in our manuscript.

Hansen et al. described that the optimal m/z width for data binning during this filtering step must be "determined by the mass resolution in such a way that two close, but separate mass peaks will not be mixed together", by applying a weighted polynomial filtering method (Metabolomics 2007 3:41). If this m/z value is increased "the smoothing will fit to the underlying spectrum resulting in over-fitting", while decreasing this width the "smaller peaks are gradually removed". Thereby, mass spectra from DIMS are usually binned in intervals of 0.01-0.5 Da (see Analyst 2010 135:2970; Int J Mass Spectrometry 2012 309:200; Metabolomics 2010 6:156; Int J Genomics 2014 894296). For this reason, we selected m/z width = 0.1 Da.

Furthermore, peak selection must be accompanied by a "noise elimination" step. In this work the noise level was set to 10 counts because several compounds presented very small signal intensities (principally at low m/z values, determined empirically from experimental spectra), although the use of this non-restrictive cutoff obviously leads to the inclusion of numerous spurious signals in the final data matrix. However, given that spurious signals are randomly distributed across all the samples, these peaks do not influence significantly subsequent statistical analyses.

Taking all this into account, the abovementioned sentence (line 138) has been re-written to clarify the data filtering step.

Latter on the authors use all types of mass errors:

2. Line 156: "Potential biomarkers were identified matching the experimental accurate mass". Which experimental accurate mass with 0.1 Da error?

And then: Line 160 …"characteristic ions in positive ionization mode at m/z 184.07, 104.10 and 86.09, and two typical fragments…"; they used two decimal figures, while in Tables they used three.

As stated in the response to the first question, 0.1Da is the m/z width employed for data binning (not mass error). All m/z values from the entire manuscript have been revised to display three decimals.

Chemometric models:

3. Line 147: Quality of the models was assessed by the R2 and Q2 values, supplied by the software, which provided information about the class separation and predictive power of the model, respectively. Looking at the poor clustering of groups in PCA and being an animal model, the separation of groups was very weak, which means that PLS-DA could be overfitted; the chemometric model should be validated in any of the different ways: permutation test, leaving 1/3 out, validating OPLS-DA….

Previous metabolomic works in different transgenic models of AD also reported that PCA is not able to separate study groups, being necessary the application of supervised methods such as PLS-DA (J Clin Biochem Nutr 2013 52:133, J Proteome Res 2008 7:3678). Anyway, PLS-DA models were validated using permutation tests. Permuted models showed lower R2 and Q2 values than original models, indicating that models are not overfitted. This has been mentioned in the revised manuscript

Statistics:

4. Line 151: potential biomarkers were selected according to the Variable Importance in the Projection, or VIP (a weighted sum of squares of the PLS weight, which indicates the importance of

the variable in the model), considering only variables with VIP values higher than 1.5, indicative of significant differences among groups.
VIP values should be given in the Tables, in addition Jack Knife intervals should be calculated to prove the statistical significance of variables.
Have the authors calculated p values?

Potential biomarkers were selected according to the VIP-plots with confidence intervals derived from jack-knifing, and then were statistically validated using t-test (this has been corrected in the manuscript). VIP and p-values have been appended to tables 2-4.

Other comments
5. Are there differences between male and female according to the disease?

When p-values of potential markers listed in Tables 2-4 are compared with p-values according to gender for these metabolites, we can observe that the effect of gender is much less important that the disease state (see attached figure, for data from hippocampus).

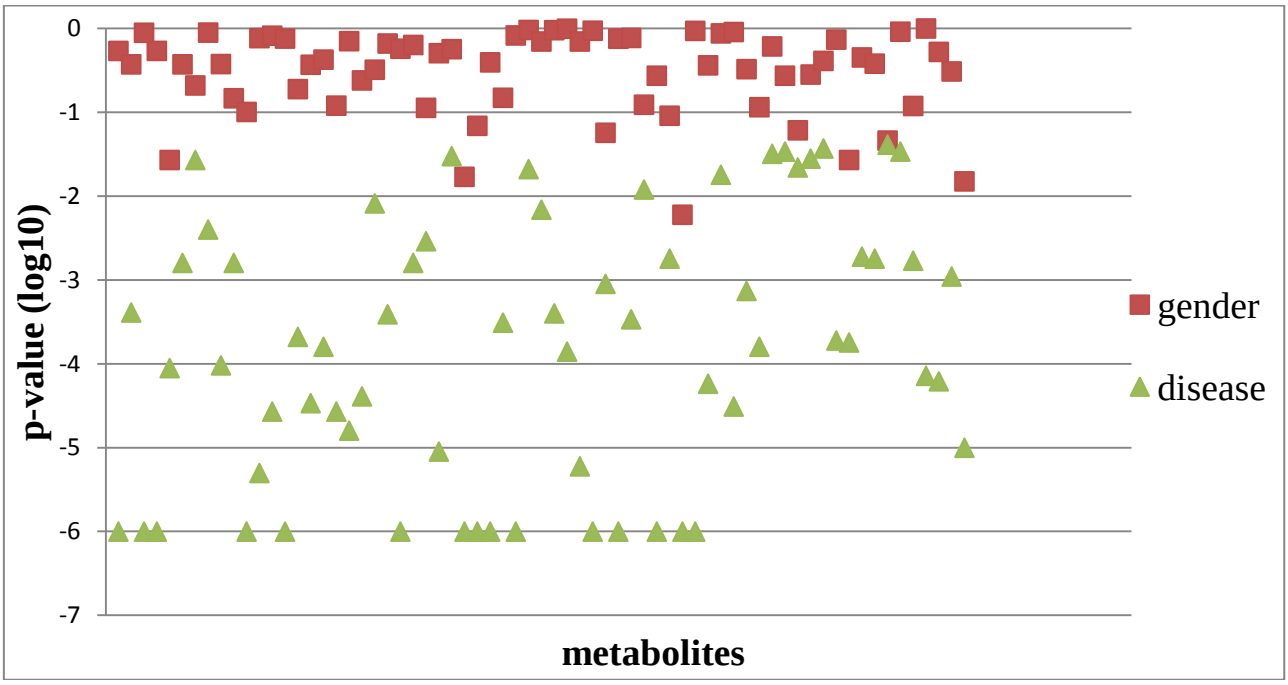

Only a few metabolites presented a statistically different trend between male and female mice (e.g. inosine, valine), in line with findings reported by van Duijn et al. (J Alzheimers Dis 2013 34:1051). However, the evaluation of gender-specific metabolic changes in the APP/PS1 model was out of the scope of this manuscript.

6. Considering that this is an analytical journal the tables should include the ions (adducts...) that lead to the identification.

Ions detected in MS/MS experiments have been appended to Tables 2-4.

Some minor mistakes in the language
7. Line 298: "transgenic mice exhibitS altered…"

It was corrected.

*Graphical Abstract

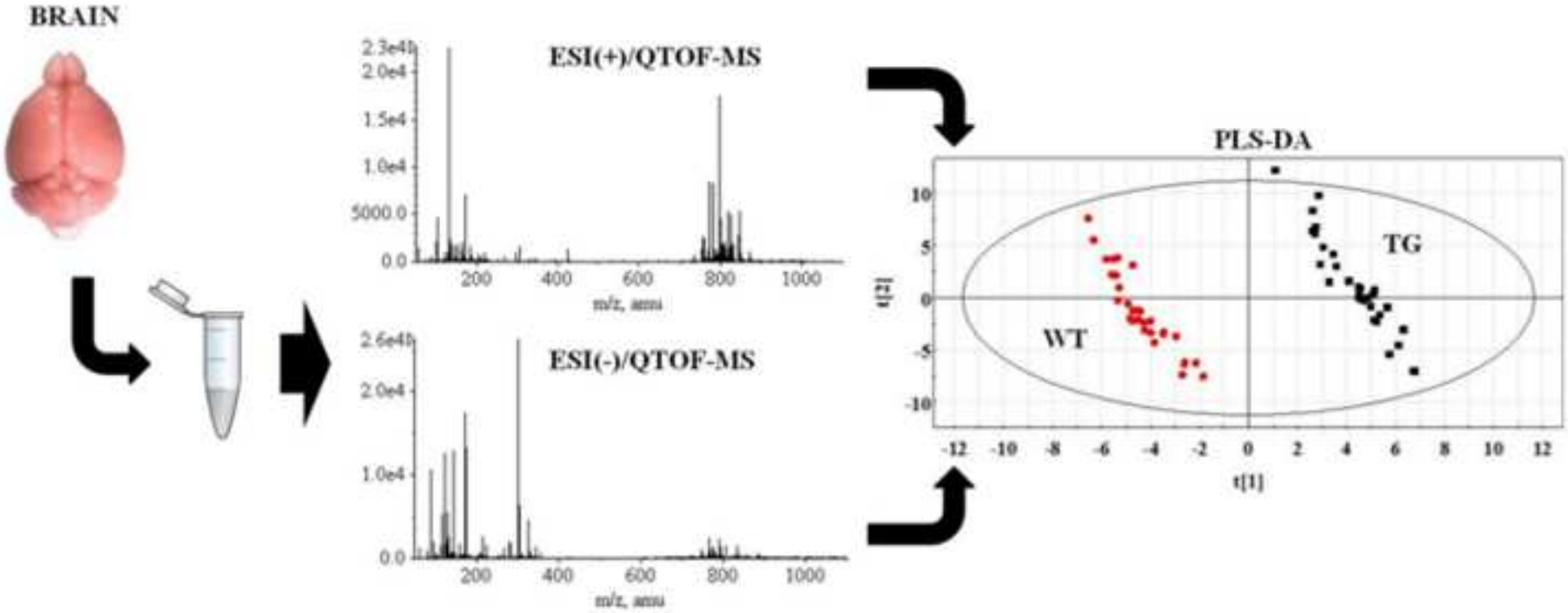

*Highlights (for review)

METABOLOMIC SCREENING OF REGIONAL BRAIN ALTERATIONS IN THE APP/PS1 TRANSGENIC MODEL OF ALZHEIMER'S DISEASE BY DIRECT INFUSION MASS SPECTROMETRY

Raúl González-Domínguez, Tamara García-Barrera, Javier Vitorica, José Luis Gómez-Ariza

- Direct infusion mass spectrometry allows a comprehensive brain metabolomic analysis
- The APP/PS1 mice exhibited an abnormal neurochemical profile compared to controls
- These failures affected hippocampus, cortex, cerebellum and olfactory bulbs
- Pathway analysis revealed multiple significant impairments in brain metabolism

METABOLOMIC SCREENING OF REGIONAL BRAIN ALTERATIONS IN THE APP/PS1 TRANSGENIC MODEL OF ALZHEIMER'S DISEASE BY DIRECT INFUSION MASS SPECTROMETRY

[a,b,c]Raúl González-Domínguez, [a,b,c]Tamara García-Barrera*, [d,e,f]Javier Vitorica, [a,b,c]José Luis Gómez-Ariza*

[a]Department of Chemistry and CC.MM. Faculty of Experimental Sciences. University of Huelva. Campus de El Carmen. 21007 Huelva. SPAIN; [b]Campus of Excellence International ceiA3. University of Huelva. SPAIN; [c]Research Center of Health and Environment (CYSMA). University of Huelva. Campus de El Carmen. 21007 Huelva. SPAIN; [d]Department Bioquímica, Bromatologia, Toxicología y Medicina Legal, Faculty of Pharmacy, University of Seville. 41012 Seville. SPAIN, [e]Centro de Investigación Biomédica en Red sobre Enfermedades Neurodegenerativas (CIBERNED). 41013 Seville. SPAIN, [f]Instituto de Biomedicina de Sevilla (IBiS)–Hospital Universitario Virgen del Rocío/CSIC/University of Seville. 41013 Seville. SPAIN

Corresponding authors:

Prof. J.L Gómez Ariza, Tel.: +34 959 219968, fax: +34 959 219942, e-mail: ariza@uhu.es

Dr. T. García-Barrera, Tel.: +34 959 219962, fax: +34 959 219942, e-mail: tamara@dqcm.uhu.es

ABSTRACT

The identification of pathological mechanisms underlying to Alzheimer's disease is of great importance for the discovery of potential markers for diagnosis and disease monitoring. In this study, we investigated regional metabolic alterations in brain from the APP/PS1 mice, a transgenic model that reproduces well some of the neuropathological and cognitive deficits observed in human Alzheimer's disease. For this purpose, hippocampus, cortex, cerebellum and olfactory bulbs were analyzed using a high-throughput metabolomic approach based on direct infusion mass spectrometry. Metabolic fingerprints showed

significant differences between transgenic and wild-type mice in all brain tissues, being hippocampus and cortex the most affected regions. Alterations in numerous metabolites were detected including phospholipids, fatty acids, purine and pyrimidine metabolites, acylcarnitines, sterols and amino acids, among others. Furthermore, metabolic pathway analysis revealed important alterations in homeostasis of lipids, energy management, and metabolism of amino acids and nucleotides. Therefore, these findings demonstrate the potential of metabolomic screening and the use of transgenic models for understanding pathogenesis of Alzheimer's disease.

KEYWORDS

Metabolomics, APP/PS1 mice, brain regions, direct infusion mass spectrometry, Alzheimer's disease

1. INTRODUCTION

Numerous transgenic mouse models of Alzheimer's disease (AD) have been developed for understanding disease pathology and testing potential therapies. The ideal model should show the full range of clinical and pathological features associated with AD, including cognitive and behavioral deficits, amyloid plaques, neurofibrillary tangles and neurodegeneration [1]. However, no existing model exhibits all these features, but each one has unique pathologies that provide insights into disease mechanisms. One of the models most extensively used is the double transgenic line APP/PS1, expressing the Swedish mutation of β-amyloid precursor protein together with deleted presenilin 1 in exon 9, which reproduces well some of the neuropathological and cognitive deficits observed in AD, with a phenotype characterized by early amyloid deposits and behavioral impairment [2]. Behavioral assessments have been traditionally used to confirm cognitive deficits in these transgenic animals [3], but they are tedious and may suffer from high individual variability. Thus, the pathophysiological status of these models is better evaluated by analysis of brain tissue samples to detect possible biomarkers. In this context, metabolomics may present a high potential for identifying neurochemical changes involved in pathological mechanisms occurring in AD, since provides a comprehensive overview of the status of organism reflecting the interactions between genes, proteins and the environment [4]. Non-invasive metabolic profiling by means of *in vivo* magnetic resonance spectroscopy (MRS) has been widely applied to AD studies in different transgenic models [5-7]. The most consistent findings observed using this approach are the decrease of N-acetyl aspartate (NAA) levels, a biomarker for neuronal integrity, and the increase of myo-inositol (mIns), which is thought to be a marker for osmotic stress or astrogliosis. Additionally, changes in other metabolites such as glutamate, creatine and choline-containing compounds were also found. On the other hand, *in vitro* nuclear magnetic resonance (NMR)-based metabolomic investigations of postmortem brain have been also proposed, providing a wider range of measurable metabolites compared to *in vivo* MRS [8-10]. However, the characterization of regional metabolomic perturbations instead of overall brain changes may be of greater interest in order to investigate the impact of disease on different brain regions and determine the most affected ones in AD-mice. In this sense, only a few authors have previously performed a comparative metabolomic study in different brain regions using NMR, demonstrating that the hippocampus and temporal cortex are the most sensitive regions to disease, but other tissues are also

affected such as cerebellum and midbrain [11-13]. Nevertheless, only medium to high abundance metabolites are detected with this approach and the identification of individual metabolites is challenging in complex mixtures, so very limited metabolic information can be obtained [14]. By contrast, mass spectrometry offers higher sensitivity and selectivity, and the potential to identify and quantify compounds. The combination of mass spectrometry with separation techniques is frequently reported in order to obtain simpler spectra and facilitate the interpretation of metabolic fingerprints. In this sense, different approaches based on liquid or gas chromatography coupled to mass spectrometry have been previously described for the characterization of metabolomic signatures associated with AD in brain from transgenic mice [15-18]. Alternatively, metabolomics based on direct infusion mass spectrometry (DIMS) has proved to be a useful screening tool due to its wide metabolome coverage and fast analysis, despite having several drawbacks such as the lack of resolution for isobars differentiation and difficulty of quantification without stable-isotope internal standards [19]. However, this high-throughput approach is not as widespread as hyphenated techniques in routine metabolomic studies, and it was only previously applied twice to address metabolic changes in hippocampus [20] and cerebellum [21] of the CRND8 transgenic mice.

This work considers the application for the first time of direct infusion electrospray mass spectrometry for the study of metabolic abnormalities in different brain regions of the APP/PS1 transgenic mice, including cortex, hippocampus, cerebellum and olfactory bulbs. Multivariate statistics demonstrated the potential of this high-throughput fingerprinting tool for the discrimination between transgenic animals and wild-type controls, and indicated that pathological processes are widespread and not only affect to hippocampus and cortex, primary targets in Alzheimer's disease. Numerous metabolites were identified as potential markers of AD-type disorders in these mice, which may contribute to deepen into underlying pathological mechanisms related to neurodegenerative processes.

2. MATERIAL AND METHODS

2.1. ANIMAL HANDLING

Transgenic APP/PS1 mice (C57BL/6 background) were generated as previously described by Jankowsky et al., expressing the Swedish mutation of APP together with PS1 deleted in exon 9 [22]. On the other hand, age-matched wild-type mice of the same genetic background (C57BL/6) were purchased from

Charles River Laboratory for their use as controls. In this study, male and female animals at 6 months of age were used for experiments (TG: N=30, male/female 13/17; WT: N=30, male/female 15/15). Animals were acclimated for 3 days after reception in rooms with a 12-h light/dark cycle at 20-25 °C, with water and food available *ad libitum*. Then, mice were anesthetized by isoflurane inhalation and sacrificed by exsanguination via cardiac puncture. Brains were rapidly removed, rinsed with saline solution (0.9% NaCl w/v) and dissected into hippocampus, cortex, cerebellum and olfactory bulbs. Finally, tissues were transferred to individual Eppendorf tubes, snap-frozen in liquid nitrogen and stored at −80 °C until analysis. Animals were handled according to the directive 2010/63/EU stipulated by the European Community, and the study was approved by the Ethical Committee of University of Huelva.

2.2. TISSUE EXTRACTION

Large brain regions (cortex and cerebellum) were cryo-homogenized using a cryogenic homogenizer SPEX SamplePrep (Freezer/Mills 6770), during 30 seconds at rate of 10 strokes per second. Then, tissues were extracted with pre-cooled 0.1% formic acid in methanol (-20ºC) using a pellet mixer for cell disruption (VWR International, UK). For this, tissue samples were exactly weighed in Eppendorf tubes (30 mg for homogenized tissues, and the entire organ for hippocampus and olfactory bulbs) and mixed with the extraction solvent (10 µl/mg). The mixture was homogenized during 2 min in an ice bath, and then centrifuged at 10000 rpm for 10 min at 4ºC. Finally, supernatant was taken for direct analysis. Furthermore, quality control (QC) samples were prepared by pooling equal volumes of each sample, which allows monitoring the stability and performance of the system along the analysis period [23].

2.3. METABOLOMIC ANALYSIS

Mass spectrometry experiments were performed in a quadrupole-time-of-flight mass spectrometry system (QTOF-MS), model QSTAR XL Hybrid system (Applied Biosystems, Foster City, CA, USA), using the electrospray (ESI) source. Samples were directly introduced into the mass spectrometer using an integrated apparatus pump and a 1000µL volume Hamilton syringe at 5 µL min^{-1} flow rate. Data were obtained in both positive and negative ionization modes, acquiring full scan spectra for 0.2 minutes in the m/z range 50-1100 with 1.005 seconds scan time. In positive mode, the ion spray voltage (IS) was set at 3300V, and high-purity nitrogen was used as curtain and nebulizer gas at flow rates about 1.13 L min^{-1} and 1.56 L min^{-1}, respectively. The source temperature was fixed at 60ºC, with a declustering potential

(DP) of 60V and a focusing potential (FP) of 250V. For ESI(-) only few parameters were modified respect ESI(+) method, with an ion spray voltage at -4000V, a declustering potential (DP) of -100V and a focusing potential (FP) of -250V. To acquire MS/MS spectra, nitrogen was used as collision gas.

2.4. DATA ANALYSIS

Metabolomic data were submitted to peak detection by Markerview™ software (Applied Biosystems) in order to filter the mass spectrometry results, and to carry out the reduction into a two-dimensional data matrix of spectral peaks and their intensities. For this, all peaks above the noise level (10 counts, determined empirically from experimental spectra) were selected and binned in intervals of 0.1Da. Finally, data were normalized according to the total area sum. Then, data were subjected to multivariate analysis by principal component analysis (PCA) and partial least squares discriminant analysis (PLS-DA) in order to compare metabolomic profiles obtained, using the SIMCA-P™ software (version 11.5, UMetrics AB, Umeå, Sweden). Before performing statistical analysis, data are usually scaled and transformed in order to minimize the technical variability between individual samples to extract the relevant biological information from these data sets [24]. For this, data was submitted to Pareto scaling, for reducing the relative importance of larger values, and logarithmic transformation, in order to approximate a normal distribution. Quality of the models was assessed by the R^2 and Q^2 values, supplied by the software, which provide information about the class separation and predictive power of the model, respectively. These parameters are ranged between 0 and 1, and they indicate the variance explained by the model for all the data analyzed (R^2) and this variance in a test set by cross-validation (Q^2). In addition, these models were validated using permutation tests (Y-scrambling) of the Y-predicted values. In Y-scrambling, class labels are randomly permuted for refitting a new model with the same number of components as the original one, and then these new models are compared with the original models to test the possibility that the original model arose by chance. Thus, an overfitted model will have similar R^2 and Q^2 to that of the randomly permuted data, while well fitted and meaningful models will have R^2 and Q^2 values higher than that of the permuted data. Finally, potential biomarkers were selected according to the Variable Importance in the Projection (VIP: a weighted sum of squares of the PLS weight, which indicates the importance of the variable in the model) with confidence intervals derived from jack-knifing. Only variables with VIP values higher than 1.5 were considered, indicative of significant

differences among groups. These metabolites were validated by t-test with Bonferroni correction for multiple testing (p-values below 0.05), using the STATISTICA 8.0 software (StatSoft, Tulsa, USA).

2.5. METABOLITES IDENTIFICATION

Potential biomarkers were identified matching the experimental accurate mass and tandem mass spectra (MS/MS) with those available in metabolomic databases (HMDB, METLIN and LIPIDMAPS). Furthermore, different classes of lipids were confirmed based on characteristic fragmentation patterns previously described. Phosphatidylcholines (PCs) and lysophosphatidylcholines (LPCs) presented characteristic ions in positive ionization mode at m/z 184.073, 104.107 and 86.096, and two typical fragments due to the loss of trimethylamine (m/z 59) and phosphocholine (m/z 183, 205 or 221, if the counterion is proton, sodium or potassium). In contrast, the product-ion spectra of ethanolamines and serines were dominated by $[M+H-141]^+$ (or $[M+Na-163]^+$ if the counterion is sodium) and $[M+H-185]^+$ respectively, arising from the elimination of the phosphoethanolamine or phosphoserine moiety. Finally, in negative mode these distinctive signals were found at 168.041, 196.038, 241.021 and $[M-H-87]^-$, for choline, ethanolamine, inositol and serine derived lipids, respectively [25]. Furthermore, the fragmentation in the glycerol backbone and release of the fatty acyl substituents enabled the identification of individual species of phospholipids, as previously described [26]. Moreover, acylcarnitines were confirmed based on characteristic fragments of 60.082 m/z identified as $[C_3H_9N+H]^+$ and 85.031 m/z identified as $[C_4H_5O_2]^+$ [27].

2.6. METABOLIC PATHWAY ANALYSIS

Metabolic pathway analysis was performed to identify and visualize the affected pathways in the APP/PS1 mice on the basis of potential biomarkers detected. For this purpose, the MetPA web tool was employed (http://metpa.metabolomics.ca), which conducts pathway analysis through pathway enrichment analysis and pathway topological analysis [28]. In this work, we select the *Mus musculus* library and use the default 'Hypergeometric Test' and 'Relative-Betweenness Centrality' algorithms for pathway enrichment analysis and pathway topological analysis, respectively. In order to identify the most relevant pathways, the impact-value threshold calculated from pathway topology analysis was set to 0.1.

3. RESULTS

Metabolomic fingerprints obtained by direct infusion mass spectrometry analysis of the different brain regions from APP/PS1 and control mice were submitted to multivariate data analysis for samples classification. As a first exploratory step, principal component analysis (PCA) was applied for a preliminary evaluation of data quality. A good clustering of quality control samples was observed in the scores plot (Fig 1A, for cortex), indicative of stability during the analyses, without significant outliers according to the Hotelling T^2-range plot. Then, partial least squares discriminant analysis (PLS-DA) was used in the same data set to sharpen the separation between groups. Scores plot displayed a clear separation between samples of transgenic (TG) and control (WT) mice, as shown in Fig 1B (for cortex). In addition, QC samples were predicted in the model and appeared clustered in the center of the scores plot, as expected since they were prepared by pooling equal volumes of individual samples. Moreover, statistical parameters confirmed the quality of these models in terms of class separation and predictive power, considering all brain regions analyzed (Table 1). In addition, the validation plots from the permutation tests (not shown) demonstrated the validity of this discrimination given that Q^2 regression showed a negative intercept and R^2 values of permuted models were lower than the R^2 value of the original one, indicating that the models were not overfitted.

Metabolites that contributed significantly to the separation of groups (VIP values higher than 1.5) were identified by MS/MS experiments. In Tables 2-4 are listed these potential markers arranged in different biochemical categories, with the ions detected in MS/MS experiments, the fold change (TG/WT ratio), p-value and VIP for each brain region. As can be observed, major changes were found in different classes of lipids including phospholipids and lysophospholipids (Table 2), acylcarnitines (Table 3), fatty acids and sterols (Table 4), but other low molecular weight metabolites were also perturbed (Table 4). Most of these metabolomic alterations were observed in hippocampus and cortex, indicating that these are the most affected brain regions in APP/PS1 mice, but several impairments were also present in cerebellum and olfactory bulbs. Moreover, pathway analysis allowed the identification of altered biochemical pathways associated with these metabolic abnormalities, revealing important impairments in metabolism of lipids, amino acids and nucleotides (Fig. 2).

4. DISCUSSION

The potential of direct infusion mass spectrometry (DIMS) for metabolomic screening has been recently demonstrated in several studies using serum and plasma samples [29-34], due to its wide metabolome coverage and fast analysis. In the present work, this approach was employed for the characterization of regional metabolic abnormalities in brain of the APP/PS1 mice, a transgenic model of Alzheimer's disease. Major differences were observed in cortex and hippocampus, but these impairments also affected other regions such as cerebellum and olfactory bulbs. Furthermore, it is also noteworthy the great number of discriminant metabolites detected with this high-throughput tool compared with previous studies based on NMR [11-13], facilitating the elucidation of potential mechanisms underlying to pathology.

The most important findings could be related to an abnormal metabolism of fatty acids, leading to the accumulation of free species principally in hippocampus and cortex (Table 4). This increase might be associated with an accelerated degradation of neural membrane lipids as well as impaired utilization of free fatty acids by β-oxidation, as revealed alterations observed in different classes of phospholipids, acylcarnitines and related compounds (Tables 2-4). Abnormal metabolism of membrane phospholipids caused by over-activated phospholipases activity, principally phospholipase A_2 (PLA_2), has been traditionally described as a key hallmark in the development of Alzheimer's disease [35]. Hydrolysis of the ester bonds from phospholipids by the action of PLA_2 produces the liberation of free fatty acids and lysophospholipids that may ultimately accumulate in brain, in agreement with results presented in Tables 2 and 4. Furthermore, different byproducts resulting from degradation of phospholipids were also elevated, including glycerophosphocholine, phosphocholine, choline, as well as the final product of this degradation process, glycerol-3-phosphate, indicating an enhanced hydrolysis of brain phosphatidylcholines in accordance with previous studies [36]. The same trend was observed for glycerophosphoinositol, which denotes that catabolic stimulation of phospholipids metabolism is not only produced in choline-containing compounds, but also occurs in other families of compounds such as phosphatidylinositols. Moreover, the release of polyunsaturated fatty acids (PUFA) from the hydrolysis of these phospholipids by PLA_2 and subsequent oxidation can explain the elevation of different eicosanoids in brain samples, such as hydroxy-eicosapentaenoic (HEPE) and hydroxy-eicosatetraenoic (HETE) acids (Table 4), which are important lipid mediators closely associated with neuronal pathways involved in AD neurobiology [37]. On the other hand, more confusing results were observed when specific changes in individual phospholipids are considered (Table 2). Alterations in phospholipids levels depended on the

type of fatty acid linked to the molecular moiety, as recently described for human AD where membrane destabilization processes were associated with imbalances in the levels of saturated/unsaturated fatty acids contained in the structure of phospholipids [33]. Thereby, major changes observed in this study corresponded to reduced levels of PUFA-containing phospholipids, principally phospatidylcholines (PC) and inositols (PI) containing docosahexaenoic acid (DHA), and most phosphatidylethanolamines (PE) and plasmenylethanolamines (PPE), which is in accordance with previous studies in brain from transgenic mice of AD [38-40]. However, a parallel accumulation of specific compounds was also observed in phospholipids derived from docosapentaenoic and docosatetraenoic acids, as well as different stearoyl-arachidonoyl-phospholipids, not previously described to our knowledge. In first place, elevated content of docosapentaenoic and docosatetraenoic acids in the brain phospholipid pool may be correlated to peroxisomal dysfunction, given that they are intermediates for the biosynthesis of long chain polyunsaturated fatty acids such as DHA in peroxisomes. In this sense, substantial peroxisome-related alterations have been previously described in AD brains, inducing the accumulation of very long chain fatty acids and deficits of plasmalogens and DHA [41]. Moreover, the increase of stearoyl-arachidonoyl-phospholipids (PC, PE, PI) denotes a profound membrane remodeling in the APP/PS1 mice as it is one of the most abundant species on the brain [42], being cortex the most affected region. Therefore, alterations in phospholipids metabolism appears to have a multifactorial origin involving over-activation of phospholipases, peroxisomal dysfunction and abnormal fatty acid composition of phospholipids.

Alternatively, deficits for most acylcarnitines in brain of the APP/PS1 mice (Table 3) might indicate a perturbed lipid metabolism, also contributing to the accumulation of free fatty acids. Lower levels of L-carnitine in brain (Table 3) have been previously reported in AD patients [43], together with altered expression of several related enzymes such as decreased carnitine acetyltransferase activity [44], or over-expressed hydroxyacyl-coenzyme A dehydrogenase (HADHA) [45] and short chain 3-hydroxyacyl-CoA dehydrogenase (SCHAD) [46]. These results suggest a perturbed transport of fatty acids into the mitochondria for β-oxidation, which together with the increased rate of phospholipids degradation finally induces the accumulation of free fatty acids. Conversely, levels of propionyl-carnitine and propionic acid were increased in brain samples, indicating a specific disturbance in propionate metabolism. In this sense, Cuadrado-Tejedor et al. recently found a differential expression of propionyl-CoA carboxylase in hippocampus of the Tg2576 mouse [47], which could cause the propionic acidemia observed in this

study. This abnormal catabolism of lipids was accompanied by other impairments in energy metabolism, regarding increased brain levels of pyruvate and alanine (Table 4). Elevation of pyruvate level in AD brain has been previously associated with a decreased rate of carbohydrate utilization by the neuron in response to drastic reductions in the activities of enzymes involved in pyruvate oxidation [48]. In the same way, increased concentration of alanine, produced in the body from the conversion of pyruvate, may also indicate a change in the carbohydrate metabolism of the brain [10-11,17]. Taking all this into account, we can conclude that several cellular impairments occur in brain of the APP/PS1 mice in direct relation to the accumulation of free fatty acids, involving multiple alterations in phospholipids metabolism and different energetic pathways, as schematized in Fig. 3A.

There is also growing evidence for the involvement of nucleotide metabolism in different neurodegenerative mechanisms in Alzheimer's disease, in accordance with alterations found for numerous purine and pyrimidine metabolites in all brain regions of the APP/PS1 mice (Table 4). Elevated adenosine monophosphate deaminase activity has been identified in AD brains, provoking accelerated degradation of AMP and over-production of ammonia leading to hyperammonemia [49]. In addition, the decrease of AMP levels may have important consequences in cellular energy homeostasis, given that it plays a central role in glucose and lipid metabolism through the AMP-activated protein kinase (AMPK), which is known to be decreased in AD brain [50]. Moreover, purinergic signaling also appears to play a role in the development of AD, with an up-regulation of adenosine receptors in the frontal cortex of affected brains [51], as well as a redistribution of these receptors, with a higher activity in neurons affected by β amyloid deposition or hyperphosphorilation of τ protein [52]. Dysregulation of pyrimidine metabolism, with decreased uridine monophosphate and increased uracil (Table 4), could reflect reduced synaptic plasticity and neuronal deficits due to decreased synthesis of phosphatidylcholines via the Kennedy cycle [53]. Finally, several studies have also implicated oxidative stress in abnormal metabolism of purines and pyrimidines in AD, demonstrating an increase of oxidized DNA bases in brain [54-55], such as 8-hydroxyadenine, 8-hydroxyguanine or FAPy-adenine, as in our metabolomic screening test. Therefore, metabolism of purines and pyrimidines highlights as a candidate pathway for the search of potential markers of pathological processes occurring in the APP/PS1 transgenic mice (Fig. 3B).

Decreased levels of cholesterol, cholesterol sulfate, deoxycholic (DCA) and taurodeoxycholic (TCA) acids were also found in hippocampus and cortex (Table 4). It has been previously demonstrated that the APP/PS1 transgenic mice exhibit altered cholesterol metabolism, resulting in reduced content of cholesterol in brain [38,56] and generating serious alterations of the physicochemical structure of lipid rafts. The same trend was observed for cholesterol sulfate, a component of cell membranes where it plays a stabilizing role [57], not previously described to our knowledge in AD research. Finally, reductions of brain deoxycholic and taurocholic acids (or isomers) could be behind different neuropathological conditions, given that ursodeoxycholic acid (UDCA) and tauroursodeoxycholic acid (TUDCA) have been demonstrated to be potent inhibitors of apoptosis [58], and they present neuroprotective action against amyloid deposition [59].

Other potential markers found by metabolomic fingerprinting of brain tissues could be related to failures in neurotransmitter systems, including deficits in tyrosine, dopamine and aspartate, as well as increased N1-acetylspermidine (Table 4). Dopamine is a neurotransmitter derived from the amino acid tyrosine, commonly linked to Parkinson's disease. However, disturbances in the biosynthesis of monoaminergic neurotransmitters and their precursors have been also reported in AD subjects [60-61]. On the other hand, aspartate is an excitatory neurotransmitter that, similarly to glutamate, usually presents lower concentrations in AD brain [18] and cerebrospinal fluid [62]. Finally, amyloid beta deposition is known to up-regulate polyamine metabolism in Alzheimer's disease by increasing ornithine decarboxylase activity and polyamine uptake [63], leading to altered levels of polyamines in brain. In this context, Inoue et al. found an abnormal increase of N1-acetylspermidine and other polyamines in AD brains, which was associated with N-methyl-D-aspartate (NMDA) receptor excitotoxicity [64], confirming our metabolomic findings. The significant reduction in urea levels (Table 4) pointed to a perturbation of the urea cycle, responsible for controlling ammonia concentrations in the organism. In Alzheimer's disease, the alteration of this pathway has been previously demonstrated on the basis of altered levels of expression in different enzymes and the corresponding genes [65]. To conclude changes observed in homocarnosine and glutathione, important antioxidants involved in the defense of the central nervous system, could be related to oxidative damage in brain. Reduced levels of homocarnosine (Table 4) have been previously described in brains of patients with Alzheimer's disease [66], as well as other related dipeptides such as carnosine [61]. On the other hand, levels of glutathione were surprisingly increased in different brain

regions of the APP/PS1 mice (Table 4), although most previous studies reported reduced content of this antioxidant during AD development in both humans and transgenic models [8,67]. However, Adams et al. also described an analogous increase in AD brain, proposing that a compensatory elevation of glutathione must occur against cellular damage produced by oxidative stress [68].

5. CONCLUSIONS

The potential of direct infusion mass spectrometry for metabolomic analysis of brain samples has been demonstrated in this study, in terms of non-targeted metabolite coverage, rapidity of analysis and, consequently, high-throughput screening capability. This approach was employed for the investigation of regional metabolic abnormalities in brain of transgenic APP/PS1 mice of Alzheimer's disease compared with wild-type control mice. Major differences were observed in hippocampus and cortex, primary brain targets in Alzheimer's disease, but cerebellum and olfactory bulbs were also affected to a lesser extent. Furthermore, these metabolic alterations could be linked to different pathways associated with pathological mechanisms occurring in the APP/PS1 mice, such as impaired metabolism of fatty acids and phospholipids, bioenergetic failures, altered metabolism of purines and pyrimidines, changes in neurotransmission or oxidative stress. Therefore, these results highlight the importance of transgenic models for the study of underlying pathological mechanisms in AD brain, a sample not readily accessible in human investigations.

Acknowledgements. This work was supported by the projects CTM2012-38720-C03-01 from the Ministerio de Ciencia e Innovación and P008-FQM-3554 and P009-FQM-4659 from the Consejería de Innovación, Ciencia y Empresa (Junta de Andalucía). Raúl González Domínguez thanks the Ministerio de Educación for a predoctoral scholarship.

REFERENCES

[1] Hall AM, Roberson ED. Mouse models of Alzheimer's disease. Brain Res Bull 2012;88:3-12.

[2] Malm T, Koistinaho J, Kanninen K. Utilization of APPswe/PS1dE9 transgenic mice in research of Alzheimer's disease: Focus on gene therapy and cell-based therapy applications. Int J Alzheimers Dis 2011;2011:517160.

[3] Filalia M, Lalonde R. Age-related cognitive decline and nesting behavior in an APPswe/PS1 bigenic model of Alzheimer's disease. Brain Res 2009;1292:93-9.

[4] Lindon JC, Holmes E, Nicholson JK. Metabonomics and its role in drug development and disease diagnosis. Expert Rev Mol Diagn 2004;4:189-99.

[5] Oberg J, Spenger C, Wang FH, Andersson A, Westman E, Skoglund P, Sunnemark D, Norinder U, Klason T, Wahlund LO, Lindberg M. Age related changes in brain metabolites observed by ^{1}H MRS in APP/PS1 mice. Neurobiol Aging 2008;29:1423-33.

[6] Xu W, Zhan Y, Huang W, Wang X, Zhang S, Lei H. Reduction of hippocampal N-acetyl aspartate level in aged APPSwe/PS1dE9 transgenic mice is associated with degeneration of CA3 pyramidal neurons. J Neurosci Res 2010;88:3155-60.

[7] Chen SQ, Cai Q, Shen YY, Wang PJ, Teng GJ, Zhang W, Zang FC. Age-related changes in brain metabolites and cognitive function in APP/PS1 transgenic mice. Behav Brain Res 2012;235:1-6.

[8] Dedeoglu A, Choi JK, Cormier K, Kowall NW, Jenkins BG. Magnetic resonance spectroscopic analysis of Alzheimer's disease mouse brain that express mutant human APP shows altered neurochemical profile. Brain Res 2004;1012:60-5.

[9] Forster DM, James MF, Williams SR. Effects of Alzheimer's disease transgenes on neurochemical expression in the mouse brain determined by ^{1}H MRS *in vitro*. NMR Biomed 2012;25:52-8.

[10] Graham SF, Holscher C, McClean P, Elliott CT, Green BD. ^{1}H NMR metabolomics investigation of an Alzheimer's disease (AD) mouse model pinpoints important biochemical disturbances in brain and plasma. Metabolomics 2013;9:974-83.

[11] Salek RM, Xia J, Innes A, Sweatman BC, Adalbert R, Randle S, McGowan E, Emson PC, Griffin JL. A metabolomic study of the CRND8 transgenic mouse model of Alzheimer's disease. Neurochem Int 2010;56:937-43.

[12] Woo DC, Lee SH, Lee DW, Kim SY, Kim GY, Rhim HS, Choi CB, Kim HY, Lee CU, Choe BY. Regional metabolic alteration of Alzheimer's disease in mouse brain expressing mutant human APP-PS1 by ^{1}H HR-MAS. Behav Brain Res 2010;211:125-31.

[13] Lalande J, Halley H, Balayssac S, Gilard V, Déjean S, Martino R, Francés B, Lassalle JM, Malet-Martino M. ^{1}H NMR metabolomic signatures in five brain regions of the AβPPswe Tg2576 mouse model of Alzheimer's disease at four ages. J Alzheimers Dis 2014;39:121-43.

[14] Dettmer K, Aronov PA, Hammock BD. Mass spectrometry-based metabolomics. Mass Spectrom Rev 2007;26:51-78.

[15] Piro JR, Benjamin DI, Duerr JM, Pi YQ, Gonzales C, Wood KM, Schwartz JW, Nomura DK, Samad TA. A dysregulated endocannabinoid-eicosanoid network supports pathogenesis in a mouse model of Alzheimer's disease. Cell Rep 2012;1:617-23.

[16] Hu ZP, Browne ER, Liu T, Angel TE, Ho PC, Chan ECY. Metabonomic profiling of TASTPM transgenic alzheimer's disease mouse model. J Proteome Res 2012;11:5903-13.

[17] Trushina E, Nemutlu E, Zhang S, ChristensenT, Camp J, Mesa J, Siddiqui A, Tamura Y, Sesaki H, Wengenack TM, Dzeja PP, Poduslo JF. Defects in mitochondrial dynamics and metabolomic signatures of evolving energetic stress in mouse models of familial Alzheimer's disease. PLoS ONE 2012;7:e32737.

[18] Wang H, Lian K, Han B, Wang Y, Kuo SH, Geng Y, Qiang J, Sun M, Wang M. Age-related alterations in the metabolic profile in the hippocampus of the senescence-accelerated mouse prone 8: a spontaneous Alzheimer's disease mouse model. J Alzheimers Dis 2014;39:841-8.

[19] Draper J, Lloyd AJ, Goodacre R, Beckmann M. Flow infusion electrospray ionisation mass spectrometry for high throughput, non-targeted metabolite fingerprinting: a review. Metabolomics 2013;9:S4-S29.

[20] Lin S, Liu H, Kanawati B, Liu L, Dong J, Li M, Huang J, Schmitt-Kopplin P, Cai Z. Hippocampal metabolomics using ultrahigh-resolution mass spectrometry reveals neuroinflammation from Alzheimer's disease in CRND8 mice. Anal Bioanal Chem 2013;405:5105-17.

[21] Lin S, Kanawati B, Liu L, Witting M, Li M, Huang J, Schmitt-Kopplin P, Cai Z. Ultra high resolution mass spectrometry-based metabolic characterization reveals cerebellum as a disturbed region in two animal models. Talanta 2014;118:45-53.

[22] Jankowsky JL, Fadale DJ, Anderson J, Xu GM, Gonzales V, Jenkins NA, Copeland NG, Lee MK, Younkin LH, Wagner SL, Younkin SG, Borchelt DR. Mutant presenilins specifically elevate the levels of the 42 residue beta-amyloid peptide in vivo: evidence for augmentation of a 42-specific g secretase. Hum Mol Genet 2004;13:159-170.

[23] Sangster T, Major H, Plumb R, Wilson AJ, Wilson ID. A pragmatic and readily implemented quality control strategy for HPLC-MS and GC-MS-based metabonomic analysis. Analyst 2006;131:1075-8.

444 [24] van den Berg RA, Hoefsloot HCJ, Westerhuis JA, Smilde AK, van der Werf MJ. Centering, scaling,
445 and transformations: improving the biological information content of metabolomics data. BMC Genomics
446 2006;7:142.
447 [25] Pulfer M, Murphy RC. Electrospray mass spectrometry of phospholipids. Mass Spectrom Rev
448 2003;22:332-64.
449 [26] Wang C, Xie S, Yang J, Yang Q, Xu G. Structural identification of human blood phospholipids using
450 liquid chromatography/quadrupole-linear ion trap mass spectrometry. Anal Chim Acta 2004;525:1-10.
451 [27] Vernez L, Hopfgartner G, Wenk M, Krahenbuhl S. Determination of carnitine and acylcarnitines in
452 urine by high-performance liquid chromatography–electrospray ionization ion trap tandem mass
453 spectrometry. J Chromatogr A 2003;984:203-13.
454 [28] Xia J, Wishart DS. MetPA: a web-based metabolomics tool for pathway analysis and visualization.
455 Bioinformatics 2010;26:2342-4.
456 [29] Lin L, Yu Q, Yan X, Hang W, Zheng J, Xing J, Huang B. Direct infusion mass spectrometry or
457 liquid chromatography mass spectrometry for human metabonomics? A serum metabonomic study of
458 kidney cancer, Analyst 2010;135:2970-8.
459 [30] Lokhov PG, Dashtiev MI, Moshkovskii SA, Archakov AI. Metabolite profiling of blood plasma of
460 patients with prostate cancer. Metabolomics 2010;6:156-63.
461 [31] Lokhov PG, Kharybin ON, Archakov AI. Diagnosis of lung cancer based on direct-infusion
462 electrospray mass spectrometry of blood plasma metabolites. Int J Mass Spectrom 2012;309:200-5.
463 [32] Gonzalez-Dominguez R, Garcia-Barrera T, Gomez-Ariza JL. Metabolomic approach to Alzheimer's
464 disease diagnosis based on mass spectrometry. Chem Papers 2012;66:829-35.
465 [33] Gonzalez-Dominguez R, Garcia-Barrera T, Gomez-Ariza JL. Combination of metabolomic and
466 phospholipid-profiling approaches for the study of Alzheimer's disease. J Proteomics 2014;104:37-47.
467 [34] González-Domínguez R, García-Barrera T, Gómez-Ariza JL. Metabolomic study of lipids in serum
468 for biomarker discovery in Alzheimer's disease using direct infusion mass spectrometry. J Pharm Biomed
469 Anal 2014, in press.
470 [35] Farooqui AA, Ong WY, Horrocks LA. Biochemical aspects of neurodegeneration in human brain:
471 involvement of neural membrane phospholipids and phospholipases A_2. Neurochem Res 2004;29:1961-
472 77.

473 [36] Walter A, Korth U, Hilgert M, Hartmann J, Weichel O, Hilgert M, Fassbender K, Schmitt A, Klein J.
474 Glycerophosphocholine is elevated in cerebrospinal fluid of Alzheimer patients. Neurobiol Aging
475 2004;25:1299-1303.
476 [37] Frisardi V, Panza F, Seripa D, Farooqui T, Farooqui AA. Glycerophospholipids and
477 glycerophospholipid-derived lipid mediators: A complex meshwork in Alzheimer's disease pathology.
478 Prog Lipid Res 2011;50:313-30.
479 [38] Yao JK, Wengenack TM, Curran GL, Poduslo JF. Reduced membrane lipids in the cortex of
480 Alzheimer's disease transgenic mice. Neurochem Res 2009;34:102-8.
481 [39] Han X, Holtzman DM, McKeel Jr DW. Plasmalogen deficiency in early Alzheimer's disease subjects
482 and in animal models: molecular characterization using electrospray ionization mass spectrometry. J
483 Neurochem 2001;77:1168-80.
484 [40] Chan RB, Oliveira TG, Cortes EP, Honig LS, Duff KE, Small SA, Wenk MR, Shui G, Di Paolo G.
485 Comparative lipidomic analysis of mouse and human brain with Alzheimer disease. J Biol Chem
486 2012;287:2678-88.
487 [41] Kou J, Kovacs GG, Höftberger R, Kulik W, Brodde A, Forss-Petter S, Hönigschnabl S, Gleiss A,
488 Brügger B, Wanders R, Just W, Budka H, Jungwirth S, Fischer P, Berger J. Peroxisomal alterations in
489 Alzheimer's disease. Acta Neuropathol 2011;122:271-83.
490 [42] Axelsen PH, Murphy RC. Quantitative analysis of phospholipids containing arachidonate and
491 docosahexaenoate chains in microdissected regions of mouse brain. J Lipid Res 2010;51:660-71.
492 [43] Graham SF, Holscher C, Green BD. Metabolic signatures of human Alzheimer's disease (AD): ^{1}H
493 NMR analysis of the polar metabolome of post-mortem brain tissue. Metabolomics 2013;in press.
494 [44] Makar TK, Cooper AJ, Tofel-Grehl B, Thaler HT, Blass JP. Carnitine, carnitine acetyltransferase,
495 and glutathione in Alzheimer brain. Neurochem Res 1995;20:705-11.
496 [45] Yao J, Hamilton RT, Cadenas E, Brinton RD. Decline in mitochondrial bioenergetics and shift to
497 ketogenic profile in brain during reproductive senescence. Biochim Biophys Acta 2010;1800:1121-6.
498 [46] Yang SY, He XY, Schulz H. 3-Hydroxyacyl-CoA dehydrogenase and short chain 3-hydroxyacyl-
499 CoA dehydrogenase in human health and disease. FEBS J 2005;272:4874-83.
500 [47] Cuadrado-Tejedor M, Cabodevilla JF, Zamarbide M, Gómez-Isla T, Franco R, Perez-Mediavilla A.
501 Age-related mitochondrial alterations without neuronal loss in the hippocampus of a transgenic model of
502 Alzheimer's disease. Curr Alzheimer Res 2013;10:390-405.

503 [48] Parnetti L, Gaiti A, Polidori MC, Brunetti M, Palumbo B, Chionne F, Cadini D, Cecchetti R, Senin
504 U. Increased cerebrospinal fluid pyruvate levels in Alzheimer's disease. Neurosci Lett 1005;199:231-3.
505 [49] Sims B, Powers RE, Sabina RL, Theibert AB. Elevated adenosine monophosphate deaminase
506 activity in Alzheimer's disease brain. Neurobiol Aging 1998;19:385-91.
507 [50] Cai Z, Yan LJ, Li K, Quazi SH, Zhao B. Roles of AMP-activated protein kinase in Alzheimer's
508 disease. Neuromol Med 2012;14:1-14.
509 [51] Albasanz JL, Perez S, Barrachina M, Ferrer I, Martín M. Up-regulation of adenosine receptors in the
510 frontal cortex in Alzheimer's disease. Brain Pathol 2008;18:211-9.
511 [52] Angulo E, Casadó V, Mallol J, Canela EI, Viñals F, Ferrer I, Lluis C, Franco R. A1 adenosine
512 receptors accumulate in neurodegenerative structures in Alzheimer's disease and mediate both amyloid
513 precursor protein processing and tau phosphorylation and translocation. Brain Pathol 2003;13:440-51.
514 [53] Czech C, Berndt P, Busch K, Schmitz O, Wiemer J, Most V, Hampel H, Kastler J, Senn H.
515 Metabolite profiling of Alzheimer's disease cerebrospinal fluid. PLoS ONE 2012;7:e31501.
516 [54] Lyras L, Cairns NJ, Jenner A, Jenner P, Halliwell B. An assessment of oxidative damage to proteins,
517 lipids, and DNA in brain from patients with Alzheimer's disease. J Neurochem 1997;68:2061-9.
518 [55] Gabbita SP, Lovell MA, Markesbery WR. Increased nuclear DNA oxidation in the brain in
519 Alzheimer's disease. J Neurochem 1998;71:2034-40.
520 [56] Fabelo N, Martín V, Marín R, Santpere G, Aso E, Ferrer I, Díaz M. Evidence for premature lipid raft
521 aging in APP/PS1 double-transgenic mice, a model of familial Alzheimer disease. J Neuropathol Exp
522 Neurol 2012;71:868-81.
523 [57] Strott CA, Higashi Y. Cholesterol sulfate in human physiology: what's it all about? J Lipid Res
524 2003;44:1268-78.
525 [58] Ramalho RM, Viana RJS, Low WC, Steer CJ, Rodrigues CMP. Bile acids and apoptosis modulation:
526 an emerging role in experimental Alzheimer's disease. Trends Mol Med 2008;14:54-62.
527 [59] Lo AC, Callaerts-Vegh Z, Nunes AF, Rodrigues CMP, D'Hooge R. Tauroursodeoxycholic acid
528 (TUDCA) supplementation prevents cognitive impairment and amyloid deposition in APP/PS1 mice.
529 Neurobiol Dis 2013;50:21-9.
530 [60] Storga D, Vrecko K, Birkmayer JGD, Reibnegger G. Monoaminergic neurotransmitters, their
531 precursors and metabolites in brains of Alzheimer patients. Neurosci Lett 1996;203:29-32.

[61] Fonteh AN, Harrington RJ, Tsai A, Liao P, Harrington MG. Free amino acid and dipeptide changes in the body fluids from Alzheimer's disease subjects. Amino Acids 2007;32:213-24.

[62] Samakashvili S, Ibáñez C, Simó C, Gil-Bea FJ, Winblad B, Cedazo-Mínguez A, Cifuentes A. Analysis of chiral amino acids in cerebrospinal fluid samples linked to different stages of Alzheimer disease. Electrophoresis 2011;32:2757-64.

[63] Yatin SM, Yatin M, Varadarajan S, Ain KB, Butterfield DA. Role of spermine in amyloid β-peptide-associated free radical-induced neurotoxicity. J Neurosci Res 2001;63:395-401.

[64] Inoue K, Tsutsui H, Akatsu H, Hashizume Y, Matsukawa N, Yamamoto T, Toyo'oka T. Metabolic profiling of Alzheimer's disease brains. Sci Rep 2013;3:2364.

[65] Hansmannel F, Sillaire A, Kamboh MI, Lendon C, Pasquier F, Hannequin D, Laumet G, Mounier A, Ayral AM, DeKosky ST, Hauw JJ, Berr C, Mann D, Amouyel P, Campion D, Lambert JC. Is the urea cycle involved in Alzheimer's disease? J Alzheimers Dis 2010;21:1013-21.

[66] Perry TL, Yong VW, Bergeron C, Hansen S, Jones K. Amino acids, glutathione, and glutathione transferase activity in the brains of patients with Alzheimer's disease. Ann Neurol 1987;21:331-6.

[67] Aoyama K, Nakaki T. Impaired glutathione synthesis in neurodegeneration. Int J Mol Sci 2013;14:21021-44.

[68] Adams JD Jr, Klaidman LK, Odunze IN, Shen HC, Miller CA. Alzheimer's and Parkinson's disease. Brain levels of glutathione, glutathione disulfide, and vitamin E. Mol Chem Neuropathol. 1991;14:213-26.

Figure captions

Fig. 1. Scores plots of PCA (A) and PLS-DA (B) models for cortex.

Fig 2. Pathway analysis overview, where each node represents an altered metabolic pathway in brain from APP/PS1 mice and its size indicates the impact of this pathway. (a) linoleic acid metabolism; (b) glycerophospholipid metabolism; (c) phenylalanine, tyrosine and tryptophan metabolism; (d) glutathione metabolism; (e) valine, leucine and isoleucine biosynthesis; (f) tyrosine metabolism; (g) pyruvate metabolism; (h) pyrimidine metabolism; (i) glycolysis or gluconeogenesis; (j) ether lipid metabolism; (k) purine metabolism.

Fig. 3. Overview of the most important metabolomic changes observed in brain from APP/PS1 mice. (A) Metabolism of phospholipids and fatty acids. (B) Metabolism of purines and pyrimidines. Abbreviations:

PL, phospholipid; PC, phosphatidylcholine; P, phosphatidylethanolamine; PPE, plasmenylethanolamine; LPL, lysophospholipid; GPC, glycerophosphocholine; GPI, glycerophosphoinositol; PC, phosphocholine; G3P. glycerol-3-phosphate; FFA, free fatty acid; acyl-Car, acylcarnitine; Ala, alanine; AMP, adenosine monophosphate; UMP, uridine monophosphate.

Table 1. Statistical parameters of PLS-DA models for hippocampus (HIP), cortex (CTX), cerebellum (CB), and olfactory bulbs (OB). A: number of latent components; R^2: variance explained; Q^2: variance predicted.

		HIP	**CTX**	**CB**	**OB**
ESI(+)/MS	**A**	3	2	2	3
	R^2	0.999	0.998	0.984	0.997
	Q^2	0.544	0.571	0.835	0.723
ESI(-)/MS	**A**	3	2	2	3
	R^2	0.998	0.988	0.992	0.999
	Q^2	0.777	0.345	0.451	0.684

585

586

587

588

589

590 **Table 2.** Lysophospholipids and phospholipids identified as potential markers for discrimination between

591 APP/PS1 and control mice. HIP, hippocampus; CTX, cortex; CB, cerebellum; OB, olfactory bulbs. FC:

592 fold change; NS: non significant change.

Metabolite	diagnostic ions	HIP		CTX		CB		OB	
		FC (p-value)	VIP	FC (p-value)	VIP	FC (p-value)	VIP	FC (p-value)	VIP
lysophospholipids									
LPE(18:1)	N: 478.300 $[M-H]^-$, 281.251, 196.038	1.28 ($1.0\cdot10^{-6}$)	2.58	NS		1.20 ($9.4\cdot10^{-4}$)	1.94	NS	
LPE(18:0)	N: 480.315 $[M-H]^-$, 283.268, 196.038	1.29 ($4.1\cdot10^{-4}$)	1.73	1.42 ($4.7\cdot10^{-5}$)	2.48	NS		NS	
LPC(16:0)	P: 496.332 $[M+H]^+$, 313.271, 184.073, 104.107, 86.096	1.19 ($2.7\cdot10^{-2}$)	1.58	1.22 ($6.0\cdot10^{-6}$)	1.83	NS		NS	
LPE(20:4)	N: 500.287 $[M-H]^-$, 303.230, 196.038	1.50 ($1.0\cdot10^{-6}$)	3.45	1.55 ($1.0\cdot10^{-6}$)	3.89	NS		NS	
LPC(18:2)	P: 558.309 $[M+K]^+$, 337.271, 184.073, 104.107, 86.096	1.22 ($4.0\cdot10^{-3}$)	1.60	NS		NS		NS	
LPC(18:1)	P: 560.304 $[M+K]^+$, 544.330 $[M+Na]^+$, 522.364 $[M+H]^+$, 339.286, 184.073, 104.107, 86.096	1.19 ($9.6\cdot10^{-5}$)	1.89	1.20 ($2.1\cdot10^{-5}$)	1.75	NS		1.24 ($1.6\cdot10^{-2}$)	2.03
LPC(18:0)	P: 562.318 $[M+K]^+$, 546.343 $[M+Na]^+$, 341.312, 184.073, 104.107, 86.096	1.15 ($1.6\cdot10^{-3}$)	1.51	1.24 ($1.0\cdot10^{-6}$)	2.06	NS		NS	
LPE(22:6)	N: 524.288 $[M-H]^-$, 327.241, 196.038	1.46 ($1.0\cdot10^{-6}$)	3.29	1.40 ($3.0\cdot10^{-6}$)	3.32	1.64 ($1.0\cdot10^{-6}$)	4.41	NS	

LPE(22:5)	N: 526.294 [M-H]$^-$, 329.252, 196.038	1.29 ($8.9\cdot10^{-5}$)	1.98	1.37 ($6.7\cdot10^{-4}$)	2.15	1.39 ($4.7\cdot10^{-4}$)	2.37	NS	
LPE(22:4)	N: 528.312 [M-H]$^-$, 331.276, 196.038	1.23 ($1.6\cdot10^{-3}$)	1.83	NS		NS		NS	
LPC(20:5)	P: 564.315 [M+Na]$^+$, 359.263, 184.073, 104.107, 86.096	1.41 ($1.0\cdot10^{-6}$)	2.99	1.46 ($1.0\cdot10^{-6}$)	2.89	1.51 ($1.2\cdot10^{-5}$)	2.98	1.34 ($2.4\cdot10^{-4}$)	2.65
LPC(20:4)	P: 582.305 [M+K]$^+$, 566.326 [M+Na]$^+$, 361.273, 184.073, 104.107, 86.096	1.26 ($5.0\cdot10^{-6}$)	2.35	1.39 ($1.0\cdot10^{-6}$)	2.42	NS		1.29 ($7.6\cdot10^{-4}$)	1.72
LPC(22:6)	P: 606.308 [M+K]$^+$, 590.327 [M+Na]$^+$, 568.348 [M+H]$^+$, 385.278, 184.073, 104.107, 86.096	1.33 ($2.7\cdot10^{-5}$)	2.23	1.36 ($2.0\cdot10^{-5}$)	2.04	1.33 ($1.5\cdot10^{-5}$)	2.34	1.22 ($6.6\cdot10^{-4}$)	1.91
LPI(20:4)	N: 619.299 [M-H]$^-$, 303.230, 241.021	1.29 ($1.0\cdot10^{-6}$)	2.60	1.39 ($1.0\cdot10^{-6}$)	3.28	NS		NS	
phospholipids									
PE(16:0/18:1)	P: 740.499 [M+Na]$^+$, 577.501, 339.286, 313.271 N: 716.532 [M-H]$^-$, 281.251, 255.237, 196.038	0.89 ($2.1\cdot10^{-4}$)	1.58	0.89 ($8.7\cdot10^{-4}$)	2.52	0.85 ($1.2\cdot10^{-4}$)	2.09	NS	
PPE(18:1/18:1)	P: 728.549 [M+H]$^+$, 587.516, 339.286 N: 726.554 [M-H]$^-$, 281.251, 196.038	0.83 ($1.6\cdot10^{-4}$)	2.00	0.78 ($4.0\cdot10^{-6}$)	2.77	NS		0.85 ($4.1\cdot10^{-3}$)	1.79
PE(18:1/18:1)	P: 766.511 [M+Na]$^+$, 603.532, 339.286 N: 742.548 [M-H]$^-$, 281.251, 196.038	0.81 ($3.4\cdot10^{-5}$)	1.82	0.82 ($2.2\cdot10^{-5}$)	2.23	0.84 ($2.1\cdot10^{-5}$)	2.21	NS	
PPE(18:1/20:4)	P: 750.529 [M+H]$^+$, 609.518, 361.273 N: 748.536 [M-H]$^-$, 303.230,	0.81 ($2.7\cdot10^{-5}$)	2.11	0.84 ($2.4\cdot10^{-4}$)	1.68	0.89 ($3.3\cdot10^{-3}$)	1.53	0.87 ($2.8\cdot10^{-3}$)	1.52

	196.038								
PE(18:0/20:4)	N: 766.549 [M-H]$^-$, 303.230, 283.269, 196.038	NS		1.14 ($6.6\cdot10^{-4}$)	1.79	NS		NS	
PC(16:0/22:6)	P: 828.569 [M+Na]$^+$, 623.497, 385.278, 313.271, 184.073, 104.107, 86.096 N: 840.539 [M+Cl]$^-$, 790.521, 327.241, 255.237, 168.041	NS		0.91 ($6.0\cdot10^{-6}$)	1.75	0.86 ($9.0\cdot10^{-5}$)	2.07	0.89 ($9.0\cdot10^{-6}$)	1.66
PC(18:0/20:4)	P: 848.542 [M+K]$^+$, 627.511, 361.273, 341.312, 184.073, 104.107, 86.096	NS		1.13 ($7.0\cdot10^{-6}$)	1.58	NS		NS	
PC(18:1/22:6)	P: 854.589 [M+Na]$^+$, 649.492, 385.278, 339.286, 184.073, 104.107, 86.096	NS		0.88 ($3.8\cdot10^{-2}$)	1.62	NS		0.86 ($5.0\cdot10^{-5}$)	1.95
PC(18:0/22:6)	P: 856.597 [M+Na]$^+$, 651.530, 385.278, 341.312, 184.073, 104.107, 86.096 N: 868.565 [M+Cl]$^-$, 818.591, 327.241, 283.269, 168.041	NS		0.86 ($2.0\cdot10^{-2}$)	1.82	0.88 ($2.8\cdot10^{-3}$)	1.77	0.83 ($1.1\cdot10^{-4}$)	2.03
PC(18:0/22:4)	P: 876.561 [M+K]$^+$, 655.538, 389.312, 341.312, 184.073, 104.107, 86.096	1.12 ($1.6\cdot10^{-5}$)	1.64	1.14 ($2.0\cdot10^{-6}$)	1.61	NS		NS	
PS(18:0/22:5)	N: 836.544 [M-H]$^-$, 749.472, 329.248, 283.269	NS		1.15 ($6.7\cdot10^{-3}$)	1.68	NS		1.18 ($3.9\cdot10^{-3}$)	1.64
PS(18:0/22:4)	N: 838.556 [M-H]$^-$, 751.503, 331.261, 283.269	1.16 ($4.1\cdot10^{-5}$)	1.86	NS		NS		NS	
PI(18:1/20:4)	N: 883.574 [M-H]$^-$, 303.230, 281.251, 241.021	NS		0.89 ($2.7\cdot10^{-2}$)	1.92	0.87 ($5.1\cdot10^{-4}$)	1.82	NS	
PI(18:0/20:4)	N: 885.563 [M-H]$^-$, 303.230, 283.269, 241.021	1.14 ($8.2\cdot10^{-3}$)	1.52	1.22 ($2.6\cdot10^{-3}$)	2.03	NS		1.26 ($1.2\cdot10^{-4}$)	2.27

Abbreviations: LPE: lysophosphoethanolamine; LPC: lysophosphocholine; LPI: lysophosphoinositol; PE: phosphoethanolamine; PPE: plasmenylethanolamine; PC: phosphocholine; PS: phosphoserine; PI: phosphoinositol, P: positive mode; N: negative mode.

622 **Table 3.** Acylcarnitines identified as potential markers for discrimination between APP/PS1 and control
623 mice. HIP, hippocampus; CTX, cortex; CB, cerebellum; OB, olfactory bulbs. FC: fold change; NS: non
624 significant change.

metabolite	diagnostic ions	HIP		CTX		CB		OB	
		FC (p-value)	VIP	FC (p-value)	VIP	FC (p-value)	VIP	FC (p-value)	VIP
carnitine	P: 162.117 $[M+H]^+$, 103.042, 85.031, 60.082, 43.019	0.89 ($3.9 \cdot 10^{-4}$)	1.52	NS		NS		NS	
acetyl-carnitine	P: 204.124 $[M+H]^+$, 145.051, 85.031, 60.082, 43.019	0.84 ($1.0 \cdot 10^{-6}$)	2.19	0.86 ($1.2 \cdot 10^{-5}$)	1.58	NS		NS	
propionyl-carnitine	P: 218.135 $[M+H]^+$, 85.031, 60.082	1.19 ($1.6 \cdot 10^{-3}$)	1.62	1.16 ($7.4 \cdot 10^{-3}$)	1.85	1.34 ($4.2 \cdot 10^{-4}$)	2.43	NS	
butyryl-carnitine	P: 232.153 $[M+H]^+$, 173.083, 85.031, 60.082	0.79 ($2.9 \cdot 10^{-3}$)	2.01	0.80 ($1.1 \cdot 10^{-3}$)	1.72	0.78 ($1.1 \cdot 10^{-3}$)	1.80	NS	
hydroxybutyryl-carnitine	P: 248.145 $[M+H]^+$, 85.031, 60.082	0.76 ($9.0 \cdot 10^{-6}$)	2.60	0.81 ($3.7 \cdot 10^{-3}$)	1.79	0.71 ($1.1 \cdot 10^{-5}$)	2.43	NS	
decanoyl-carnitine	P: 316.248 $[M+H]^+$, 85.031, 60.082	0.88 ($3.0 \cdot 10^{-2}$)	1.53	0.78 ($3.0 \cdot 10^{-2}$)	2.42	NS		NS	
myristoyl-carnitine	P: 372.313 $[M+H]^+$, 313.237, 85.031, 60.082	0.88 ($2.2 \cdot 10^{-2}$)	1.52	0.83 ($7.6 \cdot 10^{-5}$)	1.82	NS		NS	
palmitoleyl-carnitine	P: 398.322 $[M+H]^+$, 85.031, 60.082	0.73 ($1.0 \cdot 10^{-6}$)	3.03	0.69 ($1.0 \cdot 10^{-6}$)	3.13	NS		0.78 ($1.6 \cdot 10^{-5}$)	2.43
palmitoyl-carnitine	P: 400.344 $[M+H]^+$, 85.031, 60.082	0.71 ($1.0 \cdot 10^{-6}$)	3.31	0.67 ($1.0 \cdot 10^{-6}$)	3.43	0.77 ($2.7 \cdot 10^{-4}$)	2.07	0.86 ($4.2 \cdot 10^{-3}$)	1.71
oleyl-carnitine	P: 426.354 $[M+H]^+$, 85.031, 60.082	0.74 ($1.0 \cdot 10^{-6}$)	2.80	0.77 ($1.0 \cdot 10^{-6}$)	2.44	NS		NS	
stearoyl-carnitine	P: 428.367 $[M+H]^+$, 85.031, 60.082	0.78 ($3.1 \cdot 10^{-4}$)	1.65	0.74 ($1.1 \cdot 10^{-4}$)	2.45	0.68 ($4.9 \cdot 10^{-3}$)	1.87	NS	
arachidyl-carnitine	P: 456.399 $[M+H]^+$, 85.031, 60.082	0.53 ($1.0 \cdot 10^{-6}$)	4.53	0.39 ($2.3 \cdot 10^{-4}$)	4.23	0.49 ($2.8 \cdot 10^{-3}$)	3.38	0.69 ($2.4 \cdot 10^{-2}$)	1.67

625
626
627
628
629
630
631
632
633
634
635
636
637
638
639
640
641
642
643
644
645
646
647
648
649
650
651
652

653 **Table 4.** Other potential markers for discrimination between APP/PS1 and control mice. HIP,
654 hippocampus; CTX, cortex; CB, cerebellum; OB, olfactory bulbs. FC: fold change; NS: non significant
655 change.

Metabolite	diagnostic ions	HIP		CTX		CB		OB	
		FC (p-value)	VIP	FC (p-value)	VIP	FC (p-value)	VIP	FC (p-value)	VIP
fatty acids and related compounds									
palmitoleic acid	N: 253.215 $[M-H]^-$	NS		1.21 ($2.4\cdot10^{-2}$)	1.77	NS		NS	
palmitic acid	N: 255.238 $[M-H]^-$	1.18 ($2.1\cdot10^{-2}$)	1.89	1.17 ($6.8\cdot10^{-3}$)	1.85	NS		NS	
linoleic acid	N: 279.237 $[M-H]^-$	NS		1.25 ($5.8\cdot10^{-8}$)	2.56	NS		1.22 ($2.3\cdot10^{-3}$)	1.65
oleic acid	N: 281.255 $[M-H]^-$	1.18 ($6.9\cdot10^{-3}$)	1.82	1.22 ($1.4\cdot10^{-4}$)	2.31	NS		NS	
stearic acid	N: 283.268 $[M-H]^-$	1.20 ($4.0\cdot10^{-4}$)	1.96	1.17 ($2.6\cdot10^{-3}$)	1.94	NS		1.16 ($8.2\cdot10^{-4}$)	1.70
docosahexaenoic acid	N: 327.240 $[M-H]^-$	1.22 ($1.4\cdot10^{-4}$)	2.08	1.18 ($2.1\cdot10^{-3}$)	1.78	1.26 ($1.6\cdot10^{-3}$)	2.32	NS	
docosapentaenoic acid	N: 329.256 $[M-H]^-$	1.23 ($6.0\cdot10^{-6}$)	2.25	1.21 ($3.8\cdot10^{-4}$)	2.19	NS		NS	
docosatetraenoic acid	N: 331.271 $[M-H]^-$	1.41 ($1.0\cdot10^{-6}$)	3.21	1.37 ($1.0\cdot10^{-6}$)	3.26	1.35 ($9.4\cdot10^{-5}$)	2.85	1.23 ($2.8\cdot10^{-3}$)	1.97
HEPE	N: 317.222 $[M-H]^-$, 299.201, 255.212, 59.014	1.25 ($9.0\cdot10^{-4}$)	2.28	1.41 ($1.2\cdot10^{-5}$)	3.19	NS		1.56 ($1.0\cdot10^{-6}$)	3.60
HETE	N: 319.228 $[M-H]^-$, 301.209, 257.221, 59.014	1.30 ($1.0\cdot10^{-6}$)	2.67	1.33 ($4.5\cdot10^{-4}$)	2.60	1.21 ($1.1\cdot10^{-3}$)	2.18	NS	
nucleotide metabolism									
Uracil	N: 111.019 $[M-H]^-$, 42.001	1.16 ($3.4\cdot10^{-4}$)	1.68	NS		NS		1.16 ($6.2\cdot10^{-3}$)	1.51

Adenine	P: 136.063 $[M+H]^+$, 119.039, 92.028, 65.020 N: 134.048 $[M-H]^-$, 107.032, 92.030	0.93 ($1.2\cdot10^{-2}$)	2.45	0.93 ($2.7\cdot10^{-2}$)	1.78	0.83 ($1.0\cdot10^{-6}$)	2.60	0.87 ($1.6\cdot10^{-3}$)	1.60
hypoxanthine	P: 137.045 $[M+H]^+$, 119.035, 110.037, 94.041 N: 135.030 $[M-H]^-$, 92.030, 65.012	NS		NS		1.15 ($1.0\cdot10^{-6}$)	3.74	NS	
Xanthine	N: 151.023 $[M-H]^-$, 108.020, 80.028, 42.001	1.39 ($1.0\cdot10^{-6}$)	3.26	1.41 ($1.0\cdot10^{-6}$)	3.58	1.46 ($2.5\cdot10^{-2}$)	3.79	1.17 ($1.4\cdot10^{-2}$)	1.61
FAPy-adenine	P: 154.068 $[M+H]^+$, 136.061, 126.081, 119.041, 109.051	1.31 ($1.8\cdot10^{-3}$)	1.61	1.29 ($1.1\cdot10^{-4}$)	1.89	NS		NS	
Adenosine	N: 266.095 $[M-H]^-$, 134.045, 107.041	NS		NS		1.18 ($1.0\cdot10^{-6}$)	3.68	NS	
Inosine	N: 267.082 $[M-H]^-$, 135.030, 108.020	1.51 ($1.0\cdot10^{-6}$)	3.77	1.53 ($1.0\cdot10^{-6}$)	3.80	1.40 ($1.0\cdot10^{-6}$)	2.32	NS	
UMP	N: 323.033 $[M-H]^-$, 211.001, 96.970, 78.958	0.78 ($1.0\cdot10^{-6}$)	2.74	0.73 ($8.6\cdot10^{-4}$)	2.99	0.89 ($5.0\cdot10^{-5}$)	1.81	NS	
AMP	N: 346.063 $[M-H]^-$, 211.010, 134.045, 96.970, 78.958	0.85 ($5.8\cdot10^{-5}$)	1.83	0.84 ($2.0\cdot10^{-6}$)	2.27	NS		NS	
steroids									
Cholesterol	P: 369.351 $[M+H-H_2O]^+$, 287.273, 257.231, 189.162, 175.145, 161.131, 135.118, 95.082, 81.071, 57.075	0.82 ($1.8\cdot10^{-2}$)	1.72	0.74 ($1.5\cdot10^{-3}$)	2.01	NS		NS	
deoxycholic acid	P: 415.276 $[M+Na]^+$, 357.261	0.66 ($3.1\cdot10^{-5}$)	2.28	0.66 ($1.0\cdot10^{-6}$)	1.69	NS		0.83 ($1.9\cdot10^{-2}$)	1.52
taurocholic acid	P: 516.312 $[M+H]^+$, 498.288, 480.281, 462.264, 337.251	0.81 ($7.4\cdot10^{-4}$)	2.66	0.74 ($2.9\cdot10^{-3}$)	2.02	NS		NS	
cholesterol sulfate	N: 465.304 $[M-H]^-$, 96.061	0.74 ($1.6\cdot10^{-4}$)	2.80	0.77 ($3.5\cdot10^{-2}$)	2.26	NS		NS	

others											
acetic acid	N: 59.014 $[M-H]^-$, 41.012	1.19 ($3.2\cdot10^{-2}$)	1.92	NS		NS		NS			
Urea	P: 61.040 $[M+H]^+$, 44.012	0.88 ($2.8\cdot10^{-2}$)	1.60	0.69 ($2.7\cdot10^{-3}$)	2.35	NS		0.81 ($3.6\cdot10^{-3}$)	1.79		
propionic acid	N: 73.026 $[M-H]^-$, 55.017	1.23 ($3.4\cdot10^{-2}$)	2.08	NS		NS		NS			
pyruvic acid	N: 87.011 $[M-H]^-$, 43.015	1.13 ($2.2\cdot10^{-2}$)	1.70	NS		NS		NS			
Alanine	P: 90.055 $[M+H]^+$, 44.050	1.19 ($3.7\cdot10^{-2}$)	1.91	NS		NS		NS			
Choline	P: 104.105 $[M+H]^+$, 60.082	1.29 ($1.9\cdot10^{-4}$)	1.98	1.21 ($1.0\cdot10^{-6}$)	2.02	1.44 ($1.1\cdot10^{-4}$)	2.76	NS			
Valine	P: 118.084 $[M+H]^+$, 72.082, 55.055	1.15 ($1.8\cdot10^{-4}$)	1.66	1.13 ($1.1\cdot10^{-3}$)	1.76	NS		1.18 ($4.3\cdot10^{-3}$)	1.63		
aspartic acid	N: 132.032 $[M-H]^-$, 115.001, 88.041, 71.016	0.89 ($1.9\cdot10^{-3}$)	1.81	0.87 ($6.0\cdot10^{-6}$)	1.91	NS		NS			
Dopamine	N: 154.072 $[M-H]^-$, 122.037	0.92 ($1.8\cdot10^{-3}$)	2.77	0.90 ($1.8\cdot10^{-4}$)	2.93	0.77 ($2.9\cdot10^{-2}$)	2.03	0.84 ($5.5\cdot10^{-4}$)	2.07		
glycerol-3-phosphate	N: 171.008 $[M-H]^-$, 96.970, 78.958	1.19 ($4.1\cdot10^{-2}$)	1.56	1.15 ($2.9\cdot10^{-3}$)	1.52	1.16 ($2.6\cdot10^{-3}$)	1.78	NS			
Tyrosine	P: 182.085 $[M+H]^+$, 165.058, 147.046, 136.076, 123.048, 119.052	0.82 ($3.4\cdot10^{-2}$)	1.78	0.72 ($2.4\cdot10^{-2}$)	1.57	0.74 ($7.5\cdot10^{-3}$)	1.51	NS			
phosphocholine	P: 184.073 $[M+H]^+$, 104.107, 86.096	1.15 ($1.7\cdot10^{-3}$)	1.59	1.16 ($2.5\cdot10^{-3}$)	1.78	1.15 ($6.9\cdot10^{-3}$)	1.66	NS			
N1-acetylspermidine	P: 188.176 $[M+H]^+$, 171.152, 100.076, 72.081	NS		1.54 ($1.0\cdot10^{-6}$)	3.07	NS		1.26 ($1.9\cdot10^{-3}$)	1.95		
homocarnosine	P: 241.131 $[M+H]^+$, 156.078, 110.072	0.87 ($7.2\cdot10^{-5}$)	1.70	NS		NS		NS			
GPC	P: 280.091 $[M+Na]^+$, 104.107,	1.21	1.97	1.24	1.89	NS		1.22	2.11		

	86.096	($6.2\cdot10^{-5}$)		($9.0\cdot10^{-6}$)				($4.2\cdot10^{-5}$)	
Glutathione	P: 308.086 $[M+H]^+$, 233.065, 179.050, 162.025, 76.021	1.14 ($1.1\cdot10^{-3}$)	1.54	1.28 ($1.0\cdot10^{-6}$)	2.33	NS		1.24 ($2.7\cdot10^{-3}$)	1.94
GPI	N: 333.061 $[M-H]^-$, 241.021	1.21 ($1.0\cdot10^{-5}$)	2.11	1.21 ($4.8\cdot10^{-4}$)	2.00	1.19 ($3.8\cdot10^{-5}$)	2.16	1.16 ($6.2\cdot10^{-3}$)	1.63

Abbreviations: HEPE: hydroxyeicosapentaenoic acid; HETE: hydroxyeicosatetraenoic acid; UMP: uridine monophosphate; AMP: adenosine monophosphate; GPC: glycerophosphocholine; GPI: glycerophosphoinositol; P: positive mode; N: negative mode.

Figure(s)

Click here to download high resolution image

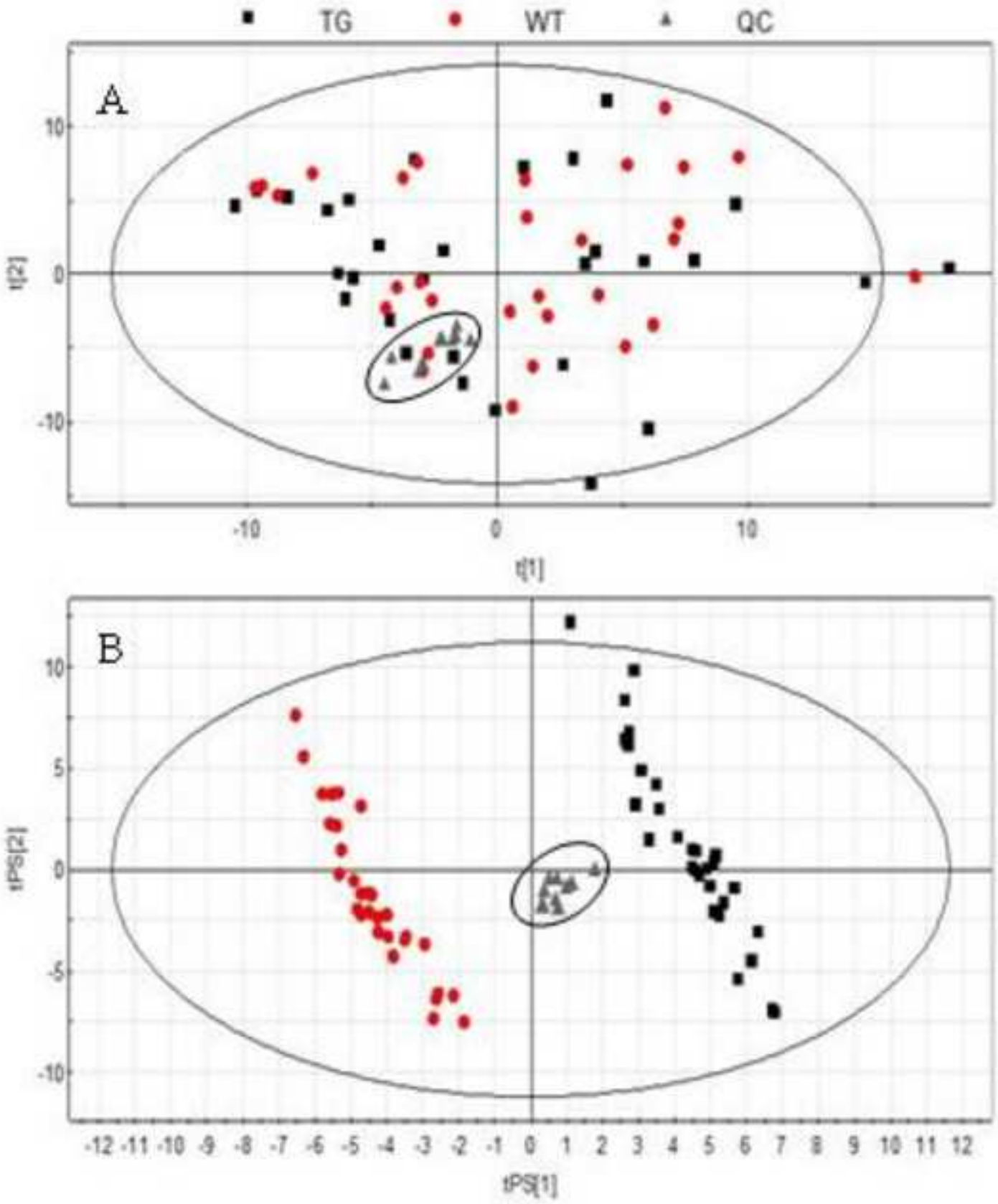

Figure(s)

Click here to download high resolution image

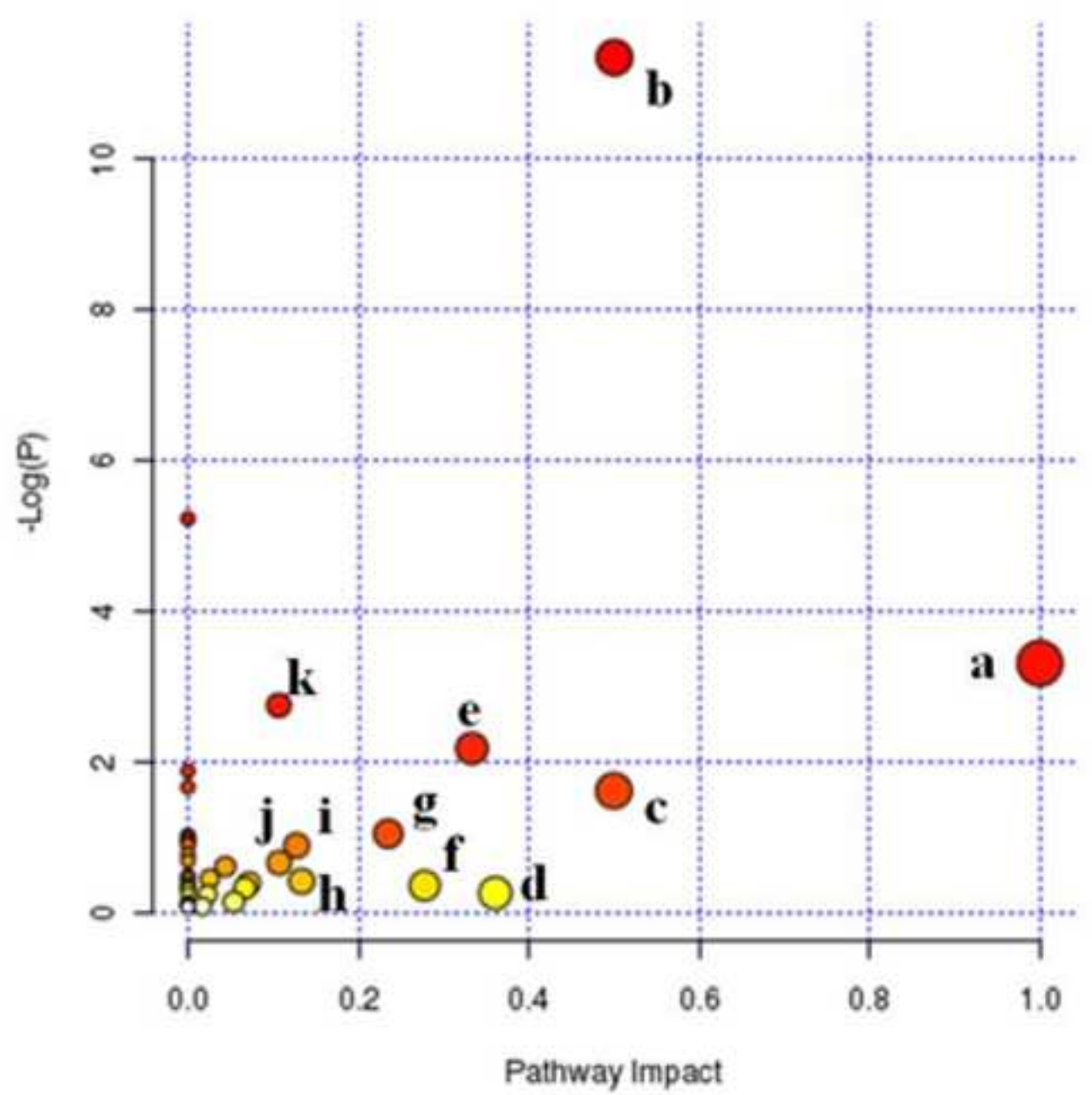

Figure(s)

Click here to download high resolution image